Published in final edited form as:
Magn Reson Imaging. 2011 July ; 29(6): 861–868. doi:10.1016/j.mri.2011.02.011.

Z Intensity-weighted Position (ZIP) Self Respiratory Gating Method for Free Breathing 3D Cardiac CINE imaging

Pascal Spincemaille, Ph.D., **Jing Liu, Ph.D.**, **Thanh Nguyen, Ph.D.**, **Martin R. Prince, M.D. Ph.D.**, and **Yi Wang, Ph.D.**
Department of Radiology Weill Medical College of Cornell University 416 East 55th Street New York, NY 10022

Abstract

A free-breathing 3D cine SSFP technique was developed using the Z Intensity weighted Position (ZIP) which is the center of mass of a projection along the slice direction as a respiratory gating signal. The ZIP signal was continuously acquired using a slice encoded k-space center sampling in every TR. The performance of this gating method was compared with a method using the k-space center signal (KC) and with conventional 2D breath-hold cine SSFP in healthy subjects by measuring image quality and left-ventricular function. The preliminary data obtained here demonstrated that the ZIP gating method provided superior respiratory motion artifact suppression when compared to the KC gating and provided left-ventricular ejection fractions, end-diastolic and end-systolic volumes similar to those obtained with the breath-hold 2D cine SSFP acquisition.

INTRODUCTION

Self-gated 2D cine balanced steady-state free precession (SSFP) imaging of the heart has been introduced as a wireless alternative to the conventional electrocardiographic (ECG) gating which is susceptible to magnetohydrodynamic interference and may cause poor image quality in cases of arrhythmia[1–4]. Self-gating has also been proposed for respiratory gating in free-breathing abdominal imaging[5] and cardiac cine imaging[6]. Typically the center of k-space is acquired at a very high temporal resolution – once per repetition time (TR) – either from the data themselves (when using radial or spiral sampling) or using a short additional readout (when using Cartesian imaging). These self-gating signals have the advantage of not interrupting the steady state, which is a concern when more traditional diaphragm navigator approaches, such as those used in segmented coronary artery MRA[7,8], are applied to 2D cine SSFP imaging of the heart[9].

There are several pitfalls associated with using the center of k-space signal (KC) for respiratory gating. It is the signal sum over all image voxels and depends heavily on slice orientation, position and thickness as well as on the exact anatomy and its movement (including flow) within the slice[10]. Therefore, the KC gating may lead to poor and inconsistent image quality as its sensitivity to motion within a slice may be highly variable. The respiratory level determined by the KC signal may also vary from slice to slice, leading

CORRESPONDING AUTHOR Pascal Spincemaille, Ph.D. Department of Radiology Weill Medical College of Cornell University 416 East 55th Street New York, NY 10022 Phone: 212 752 3936 ext 132 pas2018@med.cornell.edu.

to gaps and overlaps between successive slices due to slice misregistration similar to what may occur in standard breath-hold 2D cine imaging. Finally, a 2D acquisition generally has limited signal-to-noise ratio (SNR).

Three dimensional imaging techniques have been developed to provide higher SNR and complete coverage of the left ventricle (LV) without slice gaps and misregistration. Breath-hold 3D cine imaging typically offers limited spatial and temporal resolution[11], with better resolution obtained using radial acquisition[12,13], spiral acquisition[14], parallel imaging[15,16] or spatial-temporal undersampling techniques[17]. Free-breathing whole ventricle 3D cine acquisitions have been introduced for sagittal orientations[18] using a self-nav projection to detect motion without interrupting the steady state. The use of KC gating for free-breathing 3D cine imaging may not be straightforward, because the significantly increased slab thickness associated with 3D volumetric imaging may lead to reduced motion sensitivity of the KC signal.

The objective of this study was to investigate an alternative respiratory self-gating signal called the z intensity-weighted position (ZIP) for free-breathing 3D cine imaging of the heart. Specifically, k-space signal was acquired after the slice encoding but before the phase encoding and frequency readout in each TR, and a special view order with an inner slice encoding loop was used to generate a full k_z-encoded line per cardiac phase. After Fourier transforming this data to image space, a projection of the imaging volume onto the slice encoding axis is obtained after which the ZIP signal was calculated as the center of mass of this projection profile. The motion suppression of the KC and ZIP gating approaches were compared using 3D cine SSFP in a motion phantom and healthy volunteers. In addition, left-ventricular function measured with this approach was compared to that obtained with a routine multiple slice 2D breath-hold SSFP acquisition.

MATERIALS AND METHODS

Experiments were performed at 1.5T using a GE Signa HDx scanner (maximum gradient amplitude 33.0 mT/m, slew-rate 120 T/m/s, Excite 14M5 software version; GE Healthcare, Waukesha, WI, USA). For phantom imaging, a sphere of 10 cm radius was filled with doped water and placed on the scanner table undergoing a pre-programmed periodic motion in the head-foot direction (1 cm amplitude, 1 sec rest at both bottom and top of the motion wave form). A respiratory bellows attached to the moving scanner table detected its motion. A 3D axial slab was prescribed to completely cover the phantom. Scanning parameters were: flip angle = 50°, TR/TE = 3.7/1.2 ms, readout bandwidth = ± 62.5 kHz, FOV = 32 cm, phase FOV factor = 0.5, imaging matrix = 256×160, slice thickness = 6 mm, 32 slices and the body coil for signal reception. A partial acquisition was used in the slice direction such that 23 k_z encodings were actually acquired with zero filling to be performed before reconstruction. A synthetic trigger signal (60 BPM) was used to simulate the ECG gating signal.

Human experiments were carried out in nine normal volunteers (mean age of 29 years ± 7 standard deviation [SD]). The study protocol was approved by the Institutional Review Board and written informed consent was obtained from all subjects prior to imaging. Subjects were imaged supine using a standard eight-channel cardiac phased-array coil for signal reception, vector ECG gating for cardiac synchronization, and a respiratory bellows wrapped around the abdomen for respiratory monitoring.

Short-axis cine SSFP images of the left ventricle (LV) were acquired with both routine breath-hold 2D and free-breathing self-gated 3D sequences using the following scanning parameters: 1) 2D imaging: TR/TE = 3.6 ms/1.2 ms, flip angle = 60°, readout bandwidth =

±125 kHz, imaging matrix = 256×192, views per segment = 20, FOV = 32 cm, slice thickness = 6 mm, slice gap = 4 mm, 12–14 slices to cover the entire LV; and 2) 3D imaging: TR/TE = 4.2 ms/1.9 ms, flip angle = 50°, readout bandwidth = ±62.5 kHz, imaging matrix = 256×160, FOV = 32 cm, phase FOV factor = 0.65–0.85 depending on subject size, slice thickness = 6 mm, number of slices = 26–28 with partial k_z acquisition factor = 0.75 resulting in 19–21 actual acquired slice encodings, and image resolution 1.25×2×5 mm^3. The number of slices was chosen such that the entire LV was well within the 3D slab to counteract the lower flip angle at the edges due to imperfect RF excitation profile.

A view ordering with an inner slice encoding loop was used for both the phantom and human experiments. For each cardiac phase, all slice encodings associated with one particular phase encoding were acquired, starting with even slice encodings and followed by odd slice encodings. This was done to facilitate the data sharing method in the reconstruction for improved temporal resolution. The acquisition of cardiac phases with a constant phase encoding was repeated for a subject-specific number of R-R intervals chosen to cover an entire respiratory cycle based on the cardiac and respiratory rate reported by the scanner console (typically four to six). In each TR, one additional readout containing 30 sampling points, which were averaged to obtain a single complex value, was placed immediately after the slice refocusing and encoding gradient but before the readout pre-winder and phase encoding gradient ("Self-Nav" in Figure 1). Since all slice encodings were acquired for each cardiac phase, this allowed the repeated acquisition of the k_z axis ($k_x = k_y = 0$). After 1D Fourier transform of this line data, the projection of the entire imaging volume onto the slice axis was obtained.

Retrospective image reconstruction[19] was performed using both KC and ZIP respiratory gating signals. Given a projection profile consisting of a series of N_Z points with complex values I_z ($z = 0,\ldots, N_Z - 1$), the magnitude of the KC signal was calculated as the magnitude of the complex sum of all values along the profile $KC=\sum_{z=0}^{N_z-1} I_z$, while the ZIP signal was calculated as the center of mass of the magnitude projection profile $\mathrm{ZIP}=\sum_{z=0}^{N_z-1} z|I_z|/\sum_{z=0}^{N_z-1}|I_z|$. A KC signal can also be obtained by selecting the central k_z signal once per cardiac phase. For both KC and ZIP signals, a band pass filter was used to remove noise and cardiac motion induced signal variations as well as a very low frequency modulation (Hamming window, 0.04 & 0.5 Hz cutoff frequencies). When multiple respiratory signals were available, such as for the cardiac phased-array coil, a principal component analysis was performed and the component corresponding to the largest eigenvalue was selected as the final gating signal. This step may be seen as determining the most important common signal variation among all coil elements. From the respiratory signal, a histogram was calculated. The retrospective reconstruction selected image data acquired at the respiratory positions around the peak of this histogram and at twenty evenly distributed cardiac phases.

For image analysis, a representative mid-ventricular slice was selected. SNR for myocardium and LV blood was defined as the mean signal S_{myo} and S_{blood} within a ROI placed in the septal wall and LV cavity respectively, divided by the standard deviation σ_{air} within a ROI of background air (correction for multiple coils and sum of square reconstruction was not used since it was constant for all reconstructions). Blood-to-myocardium contrast-to-noise ratio $\mathrm{CNR}_{\mathrm{blood\text{-}myo}}$ was defined as $(S_{\mathrm{blood}}-S_{\mathrm{myo}})/\sigma_{\mathrm{air}}$. In order to account for the differences in scanning parameters between 3D and 2D acquisitions, SNR and CNR efficiency was calculated by normalizing 2D SNR and CNR by a factor equal to $\frac{\Delta_{3D}\sqrt{TS_{3D}/TR_{3D}}}{\Delta_{2D}\sqrt{TS_{2D}/TR_{2D}}}$, where Δ_{3D} and Δ_{2D} are the voxel volumes, TS_{3D} and TS_{2D} are the

readout lengths ($TS = N_x\, 2BW$ with N_x the number of readout points and BW the readout bandwidth) and TR_{3D} and TR_{2D} the repetition times for each 3D and 2D phase[20]. Statistical differences in SNR and CNR efficiency were assessed using a two-tailed paired-sample t-test. Image quality was assessed by an experienced reader using two different qualitative scores: presence of blurring (0 = severe, 1 = moderate, 2 = negligible) and the level of motion ghosting artifact suppression: 0 = none (i.e. non-diagnostic), 1 = poor, 2 = moderate, 3 = good, 4 = excellent (i.e. ghosting was absent). The statistical significance of differences in image quality scores was assessed using a two-tailed Wilcoxon paired-sample signed rank test. End diastolic volume, end systolic volume and ejection fraction was measured for all 3D and 2D cine acquisitions using LV-METRIC, a highly automated LV segmentation software[21]. A two-tailed paired-sample t-test and Bland-Altman analysis was used for assessing differences between the 2D and 3D techniques. A p-value of less than 0.05 was considered to indicate statistical significance. All values are expressed as mean ± SD.

RESULTS

Figure 2 shows 3D cine SSFP images of the motion phantom obtained with ZIP and KC gating methods. Ghosting artifacts are severe in the KC image, while they are suppressed with the ZIP method. The corresponding ZIP and KC gating signals are shown in Figure 3, where they are compared with the respiratory bellows signal (all signals are scaled to the [0, 1] range). While the ZIP signal is highly correlated with the bellows signal ($r^2 = 0.95$), the correlation between the KC signal and the bellows signal is poor ($r^2 = 0.20$).

3D CINE SSFP was obtained successfully in all subjects. The average scan time was 8.2 ± 1.1 minutes and the average heart rate 60± 8 beats per minute. Figure 4 shows an example of a systolic and diastolic frame obtained with KC gating, demonstrating severe ghosting artifacts and blurring of sharp structures such as myocardial walls and papillary muscles. On the contrary, ZIP gating provided better image quality due to the improved suppression of ghosting and blurring artifacts. Figure5 shows a portion of the ZIP and KC gating signals compared with the respiratory bellows signal as obtained for the example shown in Figure 4. Figure 6 shows another example where free-breathing 3D imaging with ZIP gating provided similar image quality to that of breath-hold 2D imaging, while 3D images obtained with KC gating suffer from motion artifacts.

Over all nine subjects, the blurring assessment score was 1.8 ± 0.4 for ZIP vs. 1.1 ± 0.3 for KC ($p = 0.031$) while the motion ghosting score was 2.9 ± 0.3 for ZIP and 2.0 ± 0.5 for KC ($p = 0.016$). The differences in end-diastolic volumes, end-systolic volumes and ejection fractions between the 2D breath-hold acquisitions and the 3D ZIP and KC reconstructions were found to be statistically non-significant (Figure 7). Bland-Altman plots comparing the 3D ZIP and KC reconstructions with the breath-hold 2D acquisition with respect to end-diastolic and end-systolic volumes and ejection fractions are shown in Figure 8, demonstrating very similar limits of agreements. Small biases in ejection fraction (<1%) were found for both 3D techniques.

Figure 9 summarizes the SNR and CNR efficiency measurements. Compared to breath-hold 2D imaging, 3D imaging with ZIP gating provided higher myocardium SNR (63.7 vs. 21.7, $p < 0.001$), as did 3D imaging with KC gating (52.5, $p = 0.015$). LV blood SNR efficiency was higher for both 3D self-gated imaging methods compared to 2D, resulting in an average increase in blood-to-myocardium CNR efficiency of 64% ($p < 0.001$) and 19% (ns) for the 3D ZIP and KC technique, respectively.

DISCUSSION

The data presented in this preliminary study demonstrate that for self-navigated free-breathing 3D cine SSFP a center of mass of the projection of the imaging volumes onto the slice axis (z intensity-weighted position, ZIP) is preferred over the k-space center signal. The ZIP gating technique provided less motion blurring and ghosting artifacts and a higher blood and myocardium SNR and CNR efficiency. Compared with breath-hold 2D cine SSFP imaging for LV assessment, free-breathing 3D imaging with KC and ZIP gating provided similar enddiastolic and end-systolic volumes and ejection fractions.

The improved motion artifact suppression is likely due to the higher sensitivity of the ZIP method to motion that takes place within the imaging volume compared to the KC signal. In a thick slab used for whole ventricle 3D coverage in the short-axis orientation, there is substantial anatomy that moves within the imaging volume. The KC signal is the signal sum of all voxels within the imaging volume and therefore provides low sensitivity to LV motion when the LV is fully encompassed by the imaging volume as is the case with whole LV 3D imaging. The ZIP method will, on the other hand, be sensitive to this kind of motion because the signal averaged z-position is detected. This was clearly seen in the phantom experiment (Figure 2) where the KC signal is not expected to change significantly for the global motion of the phantom occurring completely within the excited slab, as opposed to the center of mass ZIP method which measures the global z-displacement accurately. The corresponding derived gating signals (Figure 3) reflect this basic difference with a much higher linear correlation (r^2 = 0.95 for ZIP vs. 0.20 for KC). For in vivo imaging, the ZIP method also provided significantly improved image quality (Figure 4) as well as much higher correlation with the bellows signal (Figure5) compared to the KC gating, indicating better sensitivity to breathing motion for thick slab imaging.

The center-of-mass method was previously used in free-breathing or self-cardiac-gated techniques for radial imaging using the imaging projections themselves[3,22], where radial projections are acquired repetitively in every cardiac cycle, or in sagittal acquisitions, in which the superior-inferior readouts are available for motion detection[18]. For general orientation Cartesian sampling, such projections along the motion axis are not available. Some techniques, therefore, have added one extra signal readout within each TR to sample the center of k-space only[4]. An alternative approach consists of periodically inserting specialized readouts into the SSFP signal train for which least squares or maximum correlation coefficients are then used to detect motion[23,24]. The ZIP method proposed here can detect the z-value of the center of mass without using extra projections, whose gradients may cause eddy current artifacts in SSFP. Among the volunteers in this study, the short-axis orientation forms an angle of 53°± 14° with the superior-inferior direction – the direction of the primary component of the respiration induced motion of the heart – leading to good motion sensitivity. In addition to the center of mass, more sophisticated motion extraction algorithms such as the least squares matching used for conventional navigator echoes[25] may be used for more accurate motion detection from projection profiles.

The ZIP method relies on a repeated sampling of all slice encodings throughout the scan. In the current implementation, this is done using a linear view order with the slice encoding on the inner loop. As a result, the temporal resolution of the ZIP signal is equal to the temporal resolution of the imaging data. In order to increase the temporal resolution of the imaging data, this view order can be modified to acquire in one RR interval only even and odd slice encodings in even and odd cardiac phases respectively while acquiring the other slice encodings in another RR interval. Since the ZIP signal can be acquired independently from the phase encoding, the temporal resolution of the ZIP signal remains the same as before,

while that of the imaging data is doubled. This would allow a high temporal resolution for CINE imaging even for a large number of slices.

We have shown the feasibility of the ZIP method for respiratory gating of 3D SSFP cardiac cine imaging in the short-axis orientation. A major advantage of 3D acquisition over standard 2D breath-hold imaging is contiguous spatial coverage at higher SNR without slice misregistration. Although similar resolution and coverage can be achieved in a single ~21s breath-hold using a k-t accelerated approach[17], image quality will be crucially dependent on the ability of the patient to hold their breath. In contrast, the self-gating method developed here will allow free breathing acquisition, eradicating the patient compliance problem of breath-holding. The retrospective gating reconstruction method chosen in this preliminary study does not require real-time hardware capability and is easier to implement, but the 4–6 fold increase in scan time may limit its clinical utility. Due to the much increased SNR of 3D imaging, parallel imaging or the above mentioned k-t acceleration approach may be used to reduce scan time. The ZIP gating technique can be applied to non-Cartesian sampling in a straightforward manner[26], further increasing the data acquisition efficiency. Prospective or real-time respiratory gating may be used to improve both the efficiency and effectiveness of the developed ZIP gating method in suppressing motion artifacts[27]. The band-pass filtering needed to filter out noise and distinguish the cardiac from the respiratory component may be replaced by a real-time Kalman filter previously used for a prospective self respiratory gating in 2D cine SSFP acquisition of the heart[28].

Although the measured blood-to-myocardium CNR efficiency is higher for the 3D acquisition, the relative blood-to-myocardium contrast ratio, defined as $(S_{blood} - S_{myo})/S_{myo}$[20], was 2.8 ± 0.4 for 2D compared to 1.6 ± 0.3 for 3D. This is likely due to the use of thick slab 3D imaging which reduces the blood inflow effect and is consistent with previous findings[29,30]. An additional factor in the decreased contrast ratio is the lower flip angle of 50° used to satisfy SAR constraints. In this preliminary study, however, this reduced relative contrast ratio did not lead to significant differences in LV functional measurements.

In conclusion, the center of mass of the projection along the slice direction provides a better respiratory gating signal than the center of k-space magnitude, leading to a greater suppression of motion artifacts for 3D short-axis cardiac cine SSFP imaging. Furthermore, free-breathing 3D cine imaging provides similar LV functional measurements to that of conventional breath-hold 2D cine imaging.

REFERENCES

1. Spraggins TA. Wireless retrospective gating: application to cine cardiac imaging. Magn Reson Imaging. 1990; 8(6):675–81. [PubMed: 2266792]
2. Vasanawala S, Brittain JH, Sachs TS, Luk Pat GT, Meyer CM, Nishimura DG. Prospective wireless cardiac triggering. Proc. ISMRM. 1997:468.
3. Larson AC, White RD, Laub G, McVeigh ER, Li D, Simonetti OP. Self-gated cardiac cine MRI. Magn Reson Med. 2004; 51(1):93–102. [PubMed: 14705049]
4. Crowe ME, Larson AC, Zhang Q, Carr J, White RD, Li D, Simonetti OP. Automated rectilinear self-gated cardiac cine imaging. Magn Reson Med. 2004; 52(4):782–8. [PubMed: 15389958]
5. Brau AC, Brittain JH. Generalized self-navigated motion detection technique: Preliminary investigation in abdominal imaging. Magn Reson Med. 2006; 55(2):263–70. [PubMed: 16408272]
6. Larson AC, Kellman P, Arai A, Hirsch GA, McVeigh E, Li D, Simonetti OP. Preliminary investigation of respiratory self-gating for free-breathing segmented cine MRI. Magn Reson Med. 2005; 53(1):159–68. [PubMed: 15690515]
7. Wang Y, Rossman PJ, Grimm RC, Riederer SJ, Ehman RL. Navigator-echo-based real-time respiratory gating and triggering for reduction of respiration effects in three-dimensional coronary MR angiography. Radiology. 1996; 198(1):55–60. [PubMed: 8539406]

8. Li D, Kaushikkar S, Haacke EM, Woodard PK, Dhawale PJ, Kroeker RM, Laub G, Kuginuki Y, Gutierrez FR. Coronary arteries: three-dimensional MR imaging with retrospective respiratory gating. Radiology. 1996; 201(3):857–63. [PubMed: 8939242]
9. Peters DC, Nezafat R, Eggers H, Stehning C, Manning WJ. 2D free-breathing dual navigator-gated cardiac function validated against the 2D breath-hold acquisition. J Magn Reson Imaging. 2008; 28(3):773–7. [PubMed: 18777547]
10. Spincemaille, P.; Nguyen, TD.; Prince, MR.; Wang, Y. Quantitative Study of Motion Detection Performance of Center-Of-Kspace Measurements. Toronto: May. 2007 p. 1826
11. Jung BA, Hennig J, Scheffler K. Single-breathhold 3D-trueFISP cine cardiac imaging. Magn Reson Med. 2002; 48(5):921–5. [PubMed: 12418009]
12. Barger AV, Grist TM, Block WF, Mistretta CA. Single breath-hold 3D contrast-enhanced method for assessment of cardiac function. Magn Reson Med. 2000; 44(6):821–4. [PubMed: 11108617]
13. Peters DC, Ennis DB, Rohatgi P, Syed MA, McVeigh ER, Arai AE. 3D breath-held cardiac function with projection reconstruction in steady state free precession validated using 2D cine MRI. J Magn Reson Imaging. 2004; 20(3):411–6. [PubMed: 15332248]
14. Kressler B, Spincemaille P, Nguyen TD, Cheng L, Xi Hai Z, Prince MR, Wang Y. Three-dimensional cine imaging using variable-density spiral trajectories and SSFP with application to coronary artery angiography. Magn Reson Med. 2007; 58(3):535–43. [PubMed: 17763360]
15. Rettmann DW, Saranathan M, Wu KC, Azevedo CF, Bluemke DA, Foo TK. High temporal resolution breathheld 3D FIESTA CINE imaging: validation of ventricular function in patients with chronic myocardial infarction. J Magn Reson Imaging. 2007; 25(6):1141–6. [PubMed: 17520725]
16. Mascarenhas NB, Muthupillai R, Cheong B, Pereyra M, Flamm SD. Fast 3D cine steady-state free precession imaging with sensitivity encoding for assessment of left ventricular function in a single breath-hold. AJR Am J Roentgenol. 2006; 187(5):1235–9. [PubMed: 17056910]
17. Kozerke S, Tsao J, Razavi R, Boesiger P. Accelerating cardiac cine 3D imaging using k-t BLAST. Magn Reson Med. 2004; 52(1):19–26. [PubMed: 15236362]
18. Uribe S, Muthurangu V, Boubertakh R, Schaeffter T, Razavi R, Hill DL, Hansen MS. Whole-heart cine MRI using real-time respiratory self-gating. Magn Reson Med. 2007; 57(3):606–13. [PubMed: 17326164]
19. Thompson RB, McVeigh ER. Cardiorespiratory-resolved magnetic resonance imaging: Measuring respiratory modulation of cardiac function. Magn Reson Med. 2006
20. Haacke, EM.; Brown, RW.; Thompson, MR.; Venkatesan, R. Magnetic Resonance Imaging - physical principles and sequence design. Wiley-Liss; New York: 1999.
21. Codella NC, Weinsaft JW, Cham MD, Janik M, Prince MR, Wang Y. Left ventricle: automated segmentation by using myocardial effusion threshold reduction and intravoxel computation at MR imaging. Radiology. 2008; 248(3):1004–12. [PubMed: 18710989]
22. Stehning C, Bornert P, Nehrke K, Eggers H, Stuber M. Free-breathing whole-heart coronary MRA with 3D radial SSFP and self-navigated image reconstruction. Magn Reson Med. 2005; 54(2):476–80. [PubMed: 16032682]
23. Lai P, Larson AC, Bi X, Jerecic R, Li D. A dual-projection respiratory self-gating technique for whole-heart coronary MRA. J Magn Reson Imaging. 2008; 28(3):612–20. [PubMed: 18777542]
24. Lai P, Larson AC, Park J, Carr JC, Li D. Respiratory self-gated four-dimensional coronary MR angiography: a feasibility study. Magn Reson Med. 2008; 59(6):1378–85. [PubMed: 18506786]
25. Wang Y, Grimm RC, Felmlee JP, Riederer SJ, Ehman RL. Algorithms for extracting motion information from navigator echoes. Magn Reson Med. 1996; 36(1):117–23. [PubMed: 8795030]
26. Liu J, Spincemaille P, Codella NC, Nguyen TD, Prince MR, Wang Y. Respiratory and cardiac self-gated free-breathing cardiac CINE imaging with multiecho 3D hybrid radial SSFP acquisition. Magn Reson Med. 63(5):1230–7. [PubMed: 20432294]
27. Du YP, McVeigh ER, Bluemke DA, Silber HA, Foo TK. A comparison of prospective and retrospective respiratory navigator gating in 3D MR coronary angiography. Int J Cardiovasc Imaging. 2001; 17(4):287–96. [PubMed: 11599868]
28. Spincemaille P, Nguyen TD, Prince MR, Wang Y. Kalman filtering for real-time navigator processing. Magn Reson Med. 2008; 60(1):158–68. [PubMed: 18581354]

29. Nehrke, K.; Stehning, C.; Börnert, P. Flow-related Problems in Whole Heart Cine Coronary MR Angiography. Seattle: May. 2006 p. 2153

30. Nezafat R, Herzka D, Stehning C, Peters DC, Nehrke K, Manning WJ. Inflow quantification in three-dimensional cardiovascular MR imaging. J Magn Reson Imaging. 2008; 28(5):1273–9. [PubMed: 18972337]

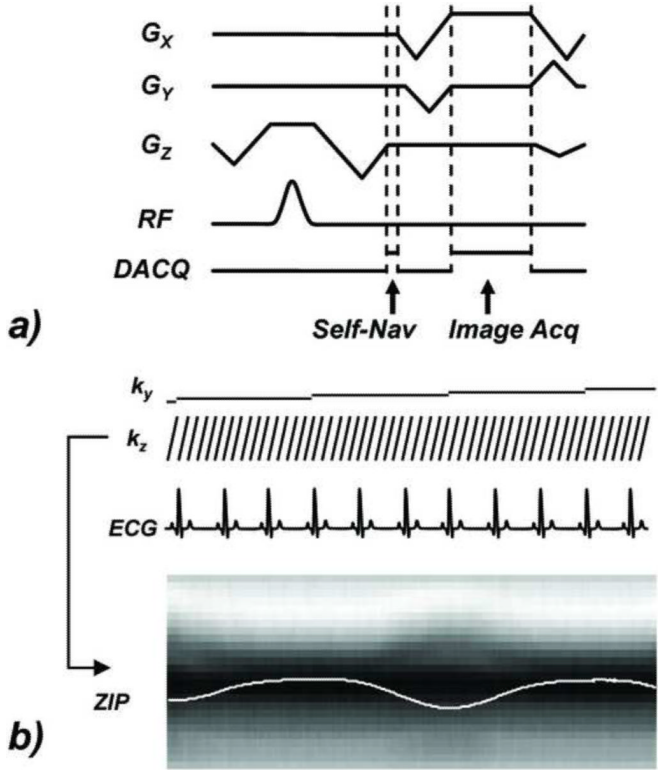

Figure 1.

Pulse sequence diagram for self-respiratory gated cine SSFP acquisition. a) the Self-Nav acquisition is positioned after the slice encoding to allow the acquisition of an entire k_z line ($k_x = k_y = 0$) in one cardiac phase. b) for each cardiac phase all slice encodings k_z are acquired simultaneous with a set of slice encoded Self-Nav data, which is then Fourier transformed to obtain a projection of the imaging volume onto the slice axis, followed by a center-of-mass calculation and a temporal band-pass filtering operation (ZIP). The phase encode (k_y) is kept constant through the entire R-R interval. In the free-breathing experiments, each phase encode k_y was acquired repeatedly during a subject-specific number of successive RR intervals (shown here is 3) for retrospective respiratory gating

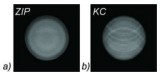

Figure 2.
Image quality comparison in a motion phantom. Severe ghosting artifacts are clearly visible in the KC reconstruction (b), but are absent using the ZIP method (a)

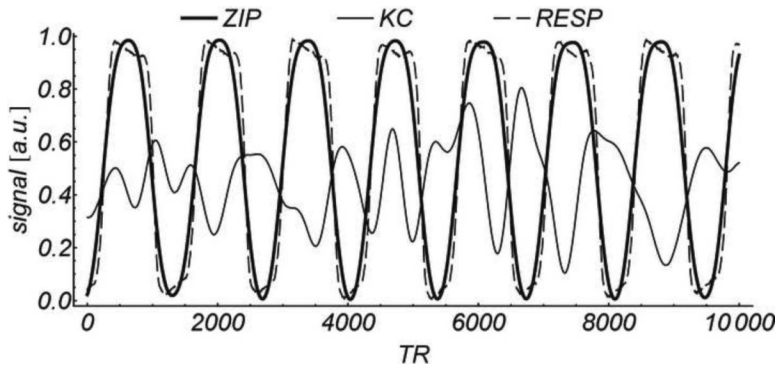

Figure 3.

Comparison of motion gating signals obtained in the motion phantom experiment Squared linear correlation with the simultaneously acquired respiratory bellows signal (RESP) was $r^2 = 0.20$ for KC vs. $r^2 = 0.95$ for ZIP. For illustrative purposes, all signals are scaled and shifted to the [0, 1] range, and only a fraction of the total waveform (10,000 TRs or about 42 sec.) is shown.

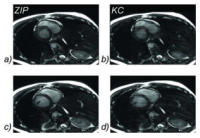

Figure 4.
Comparison of free-breathing 3D cine SSFP images obtained with KC and ZIP self-gating methods during systole (a, b) and diastole (c, d). Motion blurring and ghosting artifacts are severe with the KC gating (b, d), while they are well suppressed by the ZIP gating (a, c)

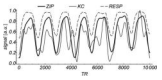

Figure 5.
Comparison of in vivo motion gating signals obtained from the example shown in Figure 4. Squared linear correlation with the simultaneously acquired respiratory bellows signal (RESP) was $r^2 = 0.36$ for KC vs. $r^2 = 0.87$ for ZIP. For illustrative purposes, all signals are scaled and shifted to the [0, 1] range, and only a fraction of the total waveform (10000 TRs or about 42 sec) is shown

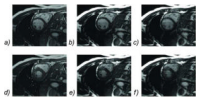

Figure 6.
Comparison of diastolic (top row) and systolic (bottom row) images obtained with breath-hold 2D cine SSFP (a, d), and free-breathing 3D cine SSFP using ZIP gating (b, e) and KC gating (c, f). KC gating produced images with severe ghosting and blurring artifacts, while ZIP gating provided images of similar quality to that of the conventional 2D breath-hold technique.

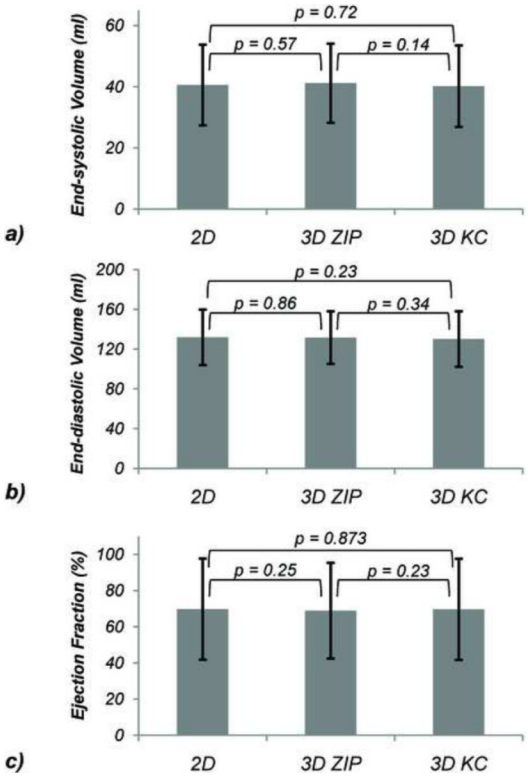

Figure 7.
Comparison of end-systolic volumes (a), end-diastolic volumes (b), and ejection fraction (c) obtained with breath-hold 2D cine SSFP (2D) and free-breathing 3D cine SSFP using ZIP and KC self-gating.

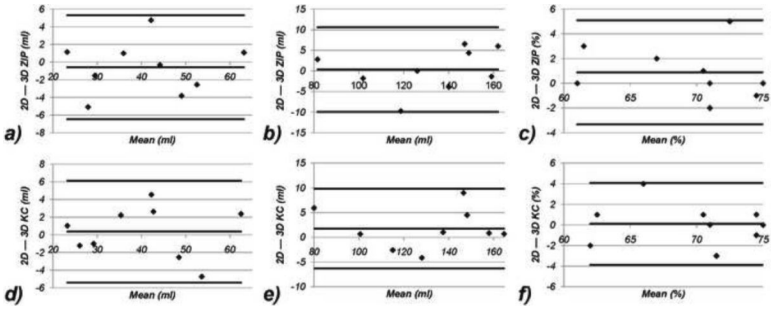

Figure 8.

Bland-Altman plots for end-diastolic volumes (a, d), end-systolic volumes (b, e) and ejection fractions (c, f) obtained with free-breathing 3D cine SSFP using ZIP (a–c) and KC (d–f) respiratory self-gating methods versus those obtained with conventional breath-hold 2D cine imaging.

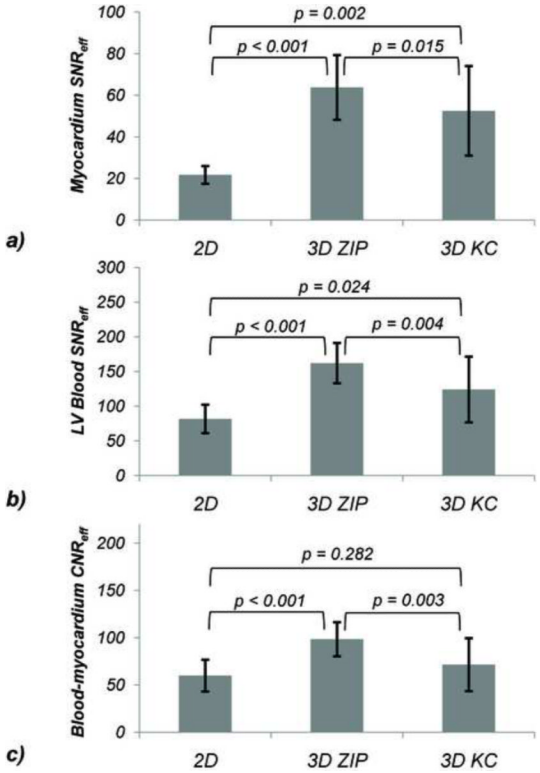

Figure 9.
Comparison of myocardium SNR efficiency of (a), LV blood SNR (b), and blood-to-myocardium CNR efficiency (c) obtained with breath-hold 2D cine SSFP and free-breathing ZIP and KC respiratory self-gated 3D cine SSFP.